

Object Detection of Satellite Images Using Multi-Channel Higher-order Local Autocorrelation

Kazuki Uehara, Hidenori Sakanashi, Hirokazu Nosato,
Masahiro Murakawa, Hiroki Miyamoto, and Ryosuke Nakamura
National Institute of Advanced Industrial Science and Technology (AIST)
1-1-1, Umezono, Tsukuba city, Ibaraki, Japan 305-8560
Email: k-uehara@aist.go.jp

Abstract—The Earth observation satellites have been monitoring the earth’s surface for a long time, and the images taken by the satellites contain large amounts of valuable data. However, it is extremely hard work to manually analyze such huge data. Thus, a method of automatic object detection is needed for satellite images to facilitate efficient data analyses. This paper describes a new image feature extended from higher-order local autocorrelation to the object detection of multispectral satellite images. The feature has been extended to extract spectral inter-relationships in addition to spatial relationships to fully exploit multispectral information. The results of experiments with object detection tasks conducted to evaluate the effectiveness of the proposed feature extension indicate that the feature realized a higher performance compared to existing methods.

I. INTRODUCTION

Earth observation satellites have been observing changes on the earth’s surface for a long time, and the collected data is utilized for various purposes, such as land-use planning, disaster support, and climate-change monitoring. However, as such data is continuously accumulated over a wide area, it is extremely hard work to manually analyze the data. Hence, techniques of automatic object-detection technique are required in order to facilitate the efficient analyses of such an enormous amount of data. In this study, we apply an image object-detection technique to the satellite images.

Satellites typically provide two types of images: a panchromatic image and multispectral images. The panchromatic image is a single tonal image that captures a wide wavelength range, including a large part of the visible spectrum with high spatial resolution. In contrast, multispectral images consist of several images that are captured using instruments that are sensitive to specific wavelengths with low spatial resolution. In general, objects have unique spectral reflection and absorption characteristics within these specific spectral bands. Multispectral images are used for obtaining spectral information which is invisible to the human eye. Moreover, image processing such as inter-channel operations is performed to emphasize the spectral characteristics to analyze satellite images using multispectral images.

© 2017 IEEE. Personal use of this material is permitted. Permission from IEEE must be obtained for all other uses, in any current or future media, including reprinting/republishing this material for advertising or promotional purposes, creating new collective works, for resale or redistribution to servers or lists, or reuse of any copyrighted component of this work in other works.

For the object detection of satellite images, the panchromatic image is usually used because of its high spatial resolution [1] [2] [3]. In contrast, Newsam and Kamath have conducted image retrieval using typical texture features, such as GLCM feature and Gabor feature, on multispectral satellite images [4]. Their results indicate that utilizing all the multispectral images taken within the visible and near-infrared bands yielded a higher performance compared to only using a panchromatic image. However, given that such features were simply connected features extracted from the respective channels, it is also necessary to take into account the relationships among channels to exploit spectral information.

In this paper, we therefore propose an image feature that considers the relationships among the channels, and evaluate the effectiveness of this feature within object-detection task experiments on satellite images. We focus on the higher-order local autocorrelation features (HLAC) [5] from the perspectives of its both calculation efficiency and recognition accuracy. HLAC is fast to compute because the feature-extraction procedure only involves product-sum operations. Thus, the feature is effective for large scale images, such as satellite images. The feature can capture the local geometric patterns of images. However, as HLAC is unable to extract the relationships among channels, we have extended it to extract those relationships in addition to the local geometric patterns.

II. SATELLITE IMAGE

Earth observation satellites are operated for monitoring of earth’s surface. Their spatial and spectral resolutions depend on purpose of applications. For example, GeoEye-1 satellite provides high spatial resolution images with 0.41m, and it can capture four spectral images within the visible and the near-infrared bands [6]. SPOT-6 and SPOT-7 satellites can capture 1.5m spatial resolution of panchromatic image and four spectral images similar to the GeoEye-1 satellite [7]. These satellites are operated for commercial use.

Landsat 8 is the latest satellite within the Landsat Project that has lasted over four decades and continues to observe the earth’s surface with a moderate spatial resolution of 15m to 100m [8]. It can capture multispectral images composed of 11 band images, including not only the visible light region, but also the near-infrared and the thermal-infrared regions, as shown in Table I.

TABLE I
SPECTRAL AND SPATIAL RESOLUTIONS OF LANDSAT 8 IMAGES.

Band	Wavelength [μm]	Resolution [m]
1 (Ultra blue)	0.43-0.45	30
2 (Visible, blue)	0.45-0.51	30
3 (Visible, green)	0.53-0.59	30
4 (Visible, red)	0.64-0.67	30
5 (Near-infrared)	0.85-0.88	30
6 (Short wavelength infrared)	1.57-1.65	30
7 (Short wavelength infrared)	2.11-2.29	30
8 (Panchromatic)	0.50-0.68	15
9 (Cirrus)	1.39-1.38	30
10 (Long wavelength infrared)	10.60-11.19	100
11 (Long wavelength infrared)	11.50-12.51	100

In this study, we use Landsat 8 because it can capture relatively more number of spectral bands than other satellites. Moreover, the Landsat image data is freely available [9], and anyone can obtain the data about two hours after the satellite has taken the images. Thus, Landsat images are useful from the perspective of practical applications.

III. PROPOSED METHOD

A. Higher-order local autocorrelation

Higher-order local autocorrelation (HLAC) features can express local geometric patterns and are robust against noise. Moreover, the feature has important characteristic relating to shift invariance and additivity. The shift invariant property makes the same feature wherever an object is within an image. Additivity is the property whereby the overall feature for multiple objects is equal to the sum of the features for each object. As location and the number of objects within an image are unspecified, these properties are desirable for object-detection tasks.

HLAC feature has been successfully applied to various applications, because of its calculation efficiency and recognition accuracy [10] [11] [12]. The feature is calculated by adding the product of the intensity of a reference point $r = (x, y)$ and predefined displacement vectors $a = (\Delta x, \Delta y)$ within local neighbors. The N th order of the HLAC feature is formulated by (1).

$$X_N(a_1, \dots, a_N) = \sum f(r)f(r+a_1) \cdots f(r+a_N) \quad (1)$$

where, $f(r)$ represents the gray level at the position r of the image. The number of expressible features X_N increases as its order increases, while its calculation cost also increases according to the order. Therefore, in calculations for practical use, the order is usually limited up to the second order.

Figure 1 shows 35 patterns of HLAC masks whose local neighbors are 3×3 . In this case, patterns that are considered to be the same by shift are excluded. In each mask, “black” represents the reference points in multiplying the values of the pixels, while “white” represents points “not required” for

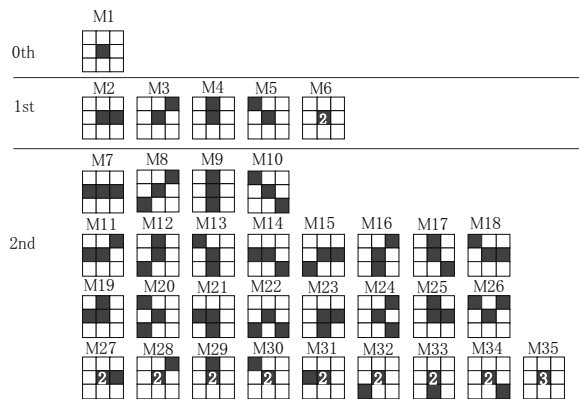


Fig. 1. HLAC mask patterns when local neighbors are 3×3 and order is limited to the second-order.

feature extraction. The numbers shown within some of the masks indicate the duplicated production of the gray level at the reference point.

In order to extract global geometric features in addition to local geometric features, the size of local neighbors can be extended by the distance between the reference point and displacement points. The size of local neighbor is defined by $(2m + 1) \times (2m + 1)$, where m (displacement distance) is an integer that is one or more. We combine multiple set of features extracted from the different size of displacement distances.

B. Multi channel extension of HLAC

Each channel of satellite image is obtained by observing the corresponding band of reflected light. In general, objects have unique spectral reflection and absorption characteristics, as shown in Fig. 2. For analysis of remote sensing images, the characteristics are usually emphasized by inter-channel operations. For example, the NDVI (Normalized Difference Vegetation Index), that is used as an indicator for the distribution and activity of vegetation, is based on the characteristic that plants absorb light in the red and reflect it in the near-infrared. The index is calculated based on the differences between two channels captured in the near-infrared and the red regions. The inter-channel operation makes the characteristic noticeable. As a result, these indices with higher value indicate dense vegetation area. In this way, the relationships among channels provide more information than obtainable from the channels independently.

Thus, we have explicitly extended the HLAC feature to extract the relationship among channels (Multi Channel HLAC: MUCHLAC). With this modification, MUCHLAC can extract not only the spatial relationships, but also the spectral relationships of reference points. In this way, the feature is capable of extracting the complicated patterns among the spectral bands.

More specifically, for first or higher orders of the HLAC, the MUCHLAC feature is computed by referring to two (or

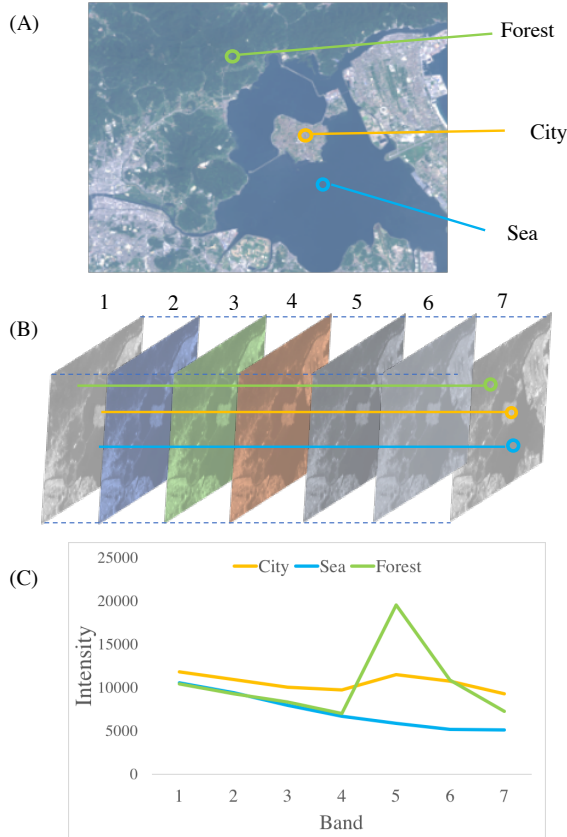


Fig. 2. (A): A color image made from visible (blue, green, red) images. (B): Multispectral images taken at each band. (C): The differences in the spectral information for the three examples of forest, city, and sea.

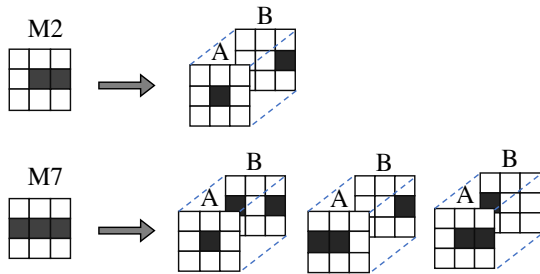


Fig. 3. Examples of the MUCHLAC mask patterns for first and second orders. Each mask pattern of the MUCHLAC is derived from each HLAC mask pattern.

more) points from different channels. Then, the product of the reference points and the displacement points are summed by scanning the entire image.

Figure 3 presents examples of MUCHLAC mask patterns combining two channels (A, B) when extracting first and second order features. The displacement point with respect to the reference point of channel A is selected from either A

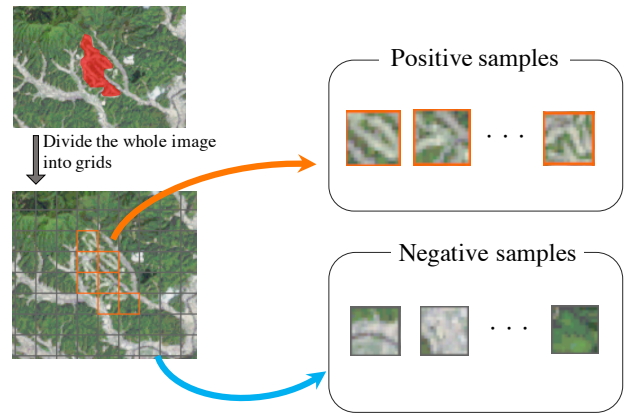


Fig. 4. An illustration of how the datasets are created. The complete image is divided into small patches. An image that includes part of a golf course is a positive sample, while one that does not is a negative sample.

or B. Here, at least one displacement point must be selected from a different channel from the one containing the reference point. Feature extraction for the other masks are the same as these examples. The number of mask patterns for MUCHLAC is five patterns in the first order and 77 patterns in the second order. Mask patterns that are equivalent in terms of shift and channel replacement are eliminated.

In the case of extracting features by combining n channels from a multi-channel image consisting of M channels, feature extraction is performed from all pairs, including the permutations of these n channels. Consequently, the number of combinations is $M P_n$. For example, MUCHLAC feature extraction from a typical color image consisting of 3 channels (RGB) is as follows: At first, the HLAC feature is extracted from each channel, respectively, and they are connected in series. Then, the MUCHLAC feature is extracted from each pair of channels considering all permutation, and it is then connected with the HLAC feature. Consequently, the length of the feature vector is $597(35 \times 3 + 82 \times 6)$.

IV. EXPERIMENT

In order to evaluate the effectiveness of the proposed feature, object-detection tasks were conducted on satellite images using both the HLAC feature, and the MUCHLAC feature. In addition, we tested the GLCM (gray level co-occurrence matrix) feature on this recognition task, because it is widely used for remote sensing images and has been shown to exhibit higher performance in [4].

A. Dataset

A satellite image is divided into a grid of patch images. The task is to recognize whether each patch image includes target object or not. We chose golf courses as the target for the task, because it encompasses considerable variations, in terms of sizes, course arrangements, and the vegetation present. The size of an image patch is 16×16 pixel. Images that include a part of a golf course are defined as positive samples, while those that do not are defined as negative samples (Fig. 4).

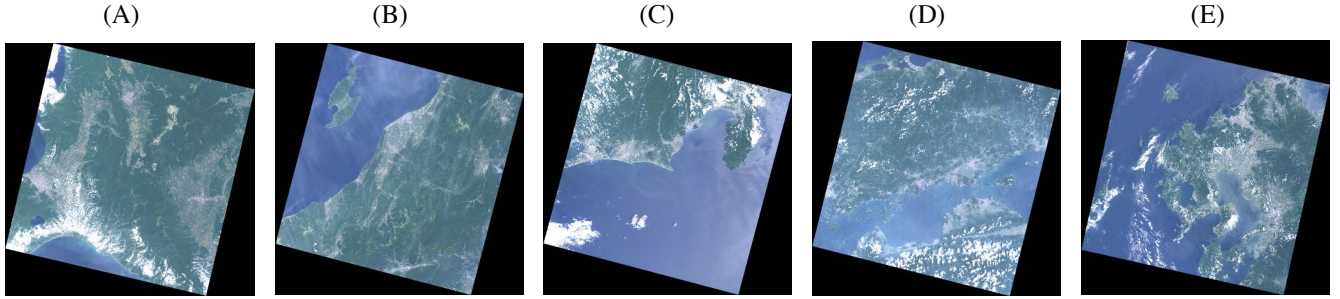


Fig. 5. The satellite images used in the experiments. The ID numbers for each satellite image are as follows, (A): LC81070302016189, (B): LC81080342015193, (C): LC81080362016196, (D): LC81110362015214, (E): LC81130372015212.

TABLE II
THE NUMBER OF SAMPLES USED IN THE EXPERIMENTS.

Image ID number	# of positives	# of negatives
LC81070302016189	610	16000
LC81080342015193	676	16000
LC81080362016196	570	16000
LC81110362015214	897	16000
LC81130372015212	697	16000

In order to create training and evaluation samples, we selected five satellite images for a part of Japan that were taken in either the July or August of 2015 and 2016 with relatively few clouds (Fig. 5). The details of the satellite images are shown in Table II. The size of each image is about 7800×8000 pixels, and each image covers approximately $170\text{km} \times 185\text{km}$.

B. Image Features

1) *MUCHLAC*: In MUCHLAC feature extraction, features are extracted for each channel and each displacement distance. Furthermore, the feature extracted by combinations between channels is concatenated. HLAC feature can be reconstructed for rotation and reflection invariance [13]. The MUCHLAC feature also can be reconstructed in an identical manner to that of the HLAC. We reconstructed the feature for rotation and reflection invariance. In order to exploit the spectral information, the feature was extracted from seven bands, which were 1, 2, 3, 4, 5, 6, and 7. The displacement distances used for feature extraction were from 1 to 4. The distances were determined by preliminary experiments¹ that yielded high detection performances of both HLAC and MUCHLAC. In addition, the number of channel combinations was set to two.

2) *HLAC*: In HLAC feature extraction, features are calculated for each channel and each displacement distance from

¹The preliminary experiments were carried out in order to determine the parameters of the features and the classifier. We investigated several different parameters applied to the object detection tasks for satellite images that were different from the images shown in Table II, with respect to both their locations and dates.

the mask patterns, and connected sequentially. After extracting the HLAC, this feature is also reconstructed for rotation and reflection invariance. The HLAC feature was extracted from seven bands and from four displacement distances from 1 to 4 similar to the MUCHLAC.

3) *Gray Level Co-occurrence Matrices*: Texture features based on the spatial dependence of pixel values [14] are popular for the analysis of remote sensing images. The feature is calculated using GLCM that tabulate how often different combinations of gray levels occur within an image. Originally, 14 quantities were proposed as the feature, but, typically, only a subset of the quantities are used. We chose the five quantities of *angular second moment*, *contrast*, *inverse different moment*, *entropy*, and *correlation*, which are the same as [4]. Moreover, the angles for calculating the GLCMs were 0° , 45° , 90° , 135° . The feature was extracted from seven bands the same as both MUCHLAC and HLAC.

C. Classifier

We used Real AdaBoost [15] for the classification of the patch images. We set the number of weak learners based on the preliminary experiment in order to enhance recognition performance.

D. Evaluation Criterion

We chose precision, recall, and the F-measure as evaluation criteria. Precision is the fraction of retrieved instances that are relevant (correctness), while recall is the fraction of relevant instances that are retrieved (completeness). The F-measure is a weighted harmonic mean of precision and recall, with a non-negative value for weight (2).

$$F\text{-measure} = \frac{(\beta^2 + 1) \cdot \text{precision} \cdot \text{recall}}{\beta^2 \cdot \text{precision} + \text{recall}} \quad (2)$$

As β is commonly set to 1, we set it to 1.

E. Results and Discussion

1) *Detection Results*: Table III presents the averages for the detection results, which were analyzed by five-fold cross validation (CV). In the table, the abbreviation TP (True Positive) is the number of samples correctly predicted as positive, FP (False Positive) is the number of negative samples that

TABLE III
DETECTION RESULTS FOR PATCH IMAGE CLASSIFICATION.

	MUCLAC (ours)	HLAC	GLCM
TP	516.8	479.2	478.2
FP	62.2	90.4	90.6
TN	15934	15905.8	15905.6
FN	172.2	209.8	210.8
Precision	0.89	0.84	0.84
Recall	0.75	0.7	0.69
F measure	0.82	0.76	0.76

are incorrectly classified as positive. Similar to TP and FP, respectively, TN (True Negative) is the number of samples correctly predicted as negative, and FN (False Negative) is the number of positive samples that are incorrectly classified as negative.

The result indicate that MUCLAC exhibited higher performance than other features, in terms of all evaluation metrics. The performance levels of the HLAC and the GLCM were almost the same in this experiment.

Each component of the MUCLAC feature is calculated from each channel and combinations of multiple channels. Thus, the MUCLAC contains all the HLAC components.

In order to verify the contribution of the feature extracted from the combinations of the multiple channels to object detection, we calculated the importance of each feature component of the MUCLAC using a Random Forest [16] [17].

The calculation of feature importance is based on the idea that, if the feature is unimportant, permuting that component will not reduce prediction accuracy. To calculate the importance of a given feature component, the values for the component are randomly permuted within out-of-bag samples that are unused for forest construction. Then, the difference in terms of prediction accuracies between before and after permutation can be used as an index of importance.

Focusing on the importance of the top 100 feature components, the feature component extracted from the combinations of multiple channels occupied 90%. From both this feature component analysis and the experimental results, clearly, feature extraction that considers the interrelationships among multiple channels is effective for the object detection of multispectral images,

2) *The number of training samples:* For remote sensing images, the set of labeled data is limited and labeling task is very time consuming due to the vast amount of data. Accordingly, it is desirable to achieve high accuracy with small amounts of data. In this study, we also investigated detection performance under scenarios where the number of training samples is reduced by some ratio. The data used for evaluation is the same as that of the previous experiment. In this experiment, five-fold CV was carried out for each ratio of the data set.

Table IV shows the average sizes of the training samples used in the experiment, and Fig. 6 presents the results of the

experiment.

As Fig. 6 illustrates, performance improved as the number of samples increased. Performance sharply increases between 2% (about 1100 samples) and 6% (about 4000 samples). For conditions with more than 6% of the data, the performance in terms of F-measure exceeded 0.7. Considering the number of positive samples which is about 170 at the 6% ratio, the performance is reasonable compared with the results achieved by using the complete set of training samples. This result indicates the system can achieve relatively high performance even with a small number of samples.

3) *The number of spectral bands:* In the case of images obtained from satellites equipped sensors with higher spectral resolution, it is possible to extract even more complicated interrelationships among the channels. However, as the number of channels increases, naturally, the number of feature dimensions also increases, which leads to increases in computational times. Thus, it is important to consider which feature components to select depending on the problem being tackled.

This sub-section reports on an additional experiment conducted to evaluate an approach to feature selection that balances reductions in the dimensions of the MUCLAC while maintaining performance. The selection procedure is as follows. First, the importance of each component is calculated using a Random Forest. Then, the components are selected in descending order of their importance.

Recognition performances for conditions of selecting between 100 to 500 components in 100 intervals are shown in Fig. 7. In this experiment, the train and the test samples are the same as those described in section IV-E1.

The figure indicates that performance drops slightly as the number of feature components is decrease. The levels of performance are constant when the number of dimensions has more than 400 components. This result suggests that most of the feature components are redundant for the detection task. Thus, it is practical to reduce the dimensions of the feature based on the importance of the feature components.

V. CONCLUSION

In this paper, we have proposed a new image feature that extends on the higher order local autocorrelation feature to extract not only spatial relationships but also spectral relationships from multi spectral satellite images. The feature is able to exploit multispectral information. In order to evaluate the effectiveness of the feature extraction, we conducted object detection task on satellite images and compared the proposed feature with existing features. As a result, the proposed feature yielded higher levels of performance than the conventional features. Moreover, we investigated a feature analysis based on the feature importance using a random forest. These results indicate that the feature extraction taking into account relationships among channels is effective for object detection of multispectral satellite images.

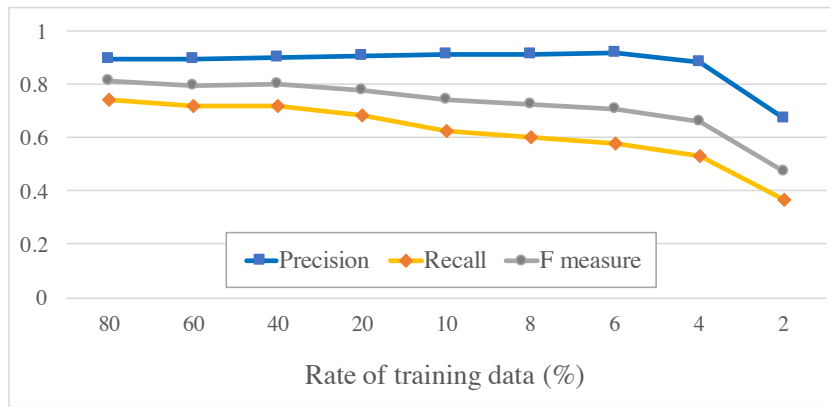


Fig. 6. Detection accuracy results as a function of reducing the training data.

TABLE IV
THE SIZE OF THE TRAINING DATA SETS USED IN THE SENSITIVITY EXPERIMENT.

Ratio (%)	80	60	40	20	10	8	6	4	2
The number of positive samples	2223.6	1675	1129.8	565.6	276.2	232.2	172.2	120.8	54.2
The number of negative samples	51199.2	38300.6	25612.6	12814.8	6387.2	5127	3879	2497.8	1055.2
Total	53422.8	39975.6	26742.4	13380.4	6663.4	5359.2	4051.2	2618.6	1109.4

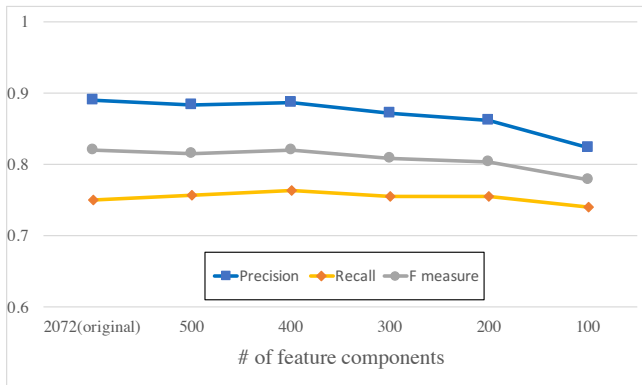


Fig. 7. Detection performance results for the MUCHLAC as a function of number of features selected.

ACKNOWLEDGMENT

This paper is based on results obtained from a project commissioned by the New Energy and Industrial Technology Development Organization (NEDO).

REFERENCES

- [1] X. Wang, B. Wang, and L. Zhang, "Airport Detection in Remote Sensing Images Based on Visual Attention", International Conference on Neural Information Processing, pp. 475-484, 2011.
- [2] X. Bai, H. Zhang, and J. Zhou, "VHR Object Detection Based on Structural Feature Extraction and Query Expansion", IEEE Transactions on Geoscience and Remote Sensing, Vol. 52, No. 10, pp. 6508-6520, 2014.
- [3] W. Zhang, X. Sun, H. Wang, and K. Fu, "A generic discriminative part-based model for geospatial object detection in optical remote sensing images", ISPRS Journal of Photogrammetry and Remote Sensing 99, pp.30-44, 2015

- [4] S. D. Newsam and C. Kamath, "Retrieval Using Texture Features in High Resolution Multi-spectral Satellite Imagery", Proceedings of the SPIE, Vol 5433, pp. 21-32, 2004.
- [5] N. Otsu and T. Kurita, "A new scheme for practical, flexible and intelligent vision systems", Proc. IAPR Workshop on Computer Vision, pp. 431-435, 1988.
- [6] C. Unsalan and K. L. Boyer, "Multispectral Satellite Image Understanding", Advances in Computer Vision and Patter Recognition, pp. 7-15, 2011.
- [7] "SPOT 6 and 7 Imagery User Guide", Astrium Services, France, 2013.
- [8] D. P. Roy, M. A. Wulder, T.R. Loveland, et al., "Landsat-8: Science and product vision for terrestrial global change research", Remote Sensing of Environment, Vol. 145, pp. 154-172, 2014.
- [9] Landsat 8 data release site, Japan, <http://landbrowser.geogrid.org/landbrowser/>
- [10] T. Nanri and N. Otsu, "Unsupervised Abnormality Detection in Video Surveillance", Conference on Machine Vision Applications, pp. 574-577, 2005.
- [11] K. Iwata, Y. Satoh, T. Kobayashi, I. Yoda and N. Otsu, "Application of the Unusual Motion Detection Using CHLAC to the Video Surveillance", International Conference on Neural Information Processing, pp. 628-636, 2007.
- [12] N. Otsu, "ARGUS: Adaptive Recognition for General Use System - Its theoretical construction and applications-", Synthesiology English edition, Vol. 4, No. 2, pp. 75-86, 2011.
- [13] H. Nosato, T. Kurihara, H. Sakanashi, et al., "An Extended Method of Higher-order Local Autocorrelation Feature Extraction for Classification of Histopathological Images", IPSJ Transactions on Computer Vision and Applications, Vol. 3, pp. 211-221, 2011.
- [14] R. M. Haralick, K. Shanmugam, and I. Dinstein, "Textural features for Image Classification", IEEE Transactions on Systems, Man and Cybernetics, Vol. SMC-3, No. 6. pp.610-621, 1973.
- [15] R. E. Schapire and Y. Singer, "Improved Boosting Algorithms Using Confidence-rated Predictions", Machine Learning, Vol. 37, pp. 297-336, 1999.
- [16] L. Breiman, "Random Forests", Machine Learning, Vol. 45, pp. 5-32, 2001.
- [17] G. Louppe, L. Wehenkel, A. Suter, and P. Geurts, "Understanding variable importances in forests of randomized trees", NIPS'13, Proceedings of the 26th International Conference on Neural Information Processing Systems, pp. 431-439, 2013.